Calculations of the distribution of trace impurities in cylindrical pores

Yu. K. Tovbin and E. V. Votyakov*

State Research Center of the Russian Federation "L. Ya. Karpov Institute of Physical Chemistry," 10 ul. Vorontsovo Pole, 103064 Moscow, Russian Federation. Fax: +7 (095) 975 2450. E-mail: tovbin@cc.nifhi.ac.ru

The equilibrium distribution of a trace impurity and the self-diffusion coefficients of molecules of the base component and the trace impurity in narrow cylindrical pores were calculated using the lattice-gas model. Two types of lattice structures with six and eight closest neighbors were considered. The sizes of the base component and impurity molecules were taken to be identical. Lateral interactions were taken into account in the quasi-chemical approximation. The equilibrium distributions of the trace impurity across a pore section in the gas and liquid phases of the base component and at the interface for the case of capillary condensation were considered. The probability of existence of isolated dimeric clusters was estimated and the self-diffusion coefficients of the base component and trace impurity for a single-phase distribution of the base component were calculated. The effects of the energy of interaction of impurities with the pore walls and the concentration of the base component on the diffusion mobility of the impurities were analyzed. The concentration dependences of the partition coefficient for the trace impurity between the pore center and the pore wall and the concentration dependences of the self-diffusion coefficients for the trace impurity molecules become nonmonotonic with an increase in the base component concentration. These effects are due to the displacement of the impurity from the near-surface area to the bulk of a pore following an increase in the pore coverage by the base component and to higher mobility of the impurity in the free bulk of the pore. Further filling of the pore bulk reduces the mobility of all molecules. The energetics of intermolecular interactions also plays a certain role.

Key words: cylindrical pores, adsorption, trace impurity, phase interface, clusters, self-diffusion coefficient, lattice-gas model, quasi-chemical approximation.

Adsorption and membrane technologies[1,2] underlie many processes of purification and separation of liquid and gas mixtures. The efficiency of fine purification of the base component from impurities is characterized by a separation factor, which is usually found from experimental data on the adsorption of a trace impurity—base component mixture on the adsorbent under study or on a membrane. However, experimental determination of these factors is a labor-consuming task; therefore, theoretical methods for calculation are significant.[3–5] Most adsorption processes occur in porous systems.[1,6,7] No experimental methods for determination of the distribution of trace impurities are known for these systems. Calculation methods seem to be the only possibility of gaining information on the distribution of trace impurities in the pores; this information can be highly important for many practical problems concerning adsorption, chromatography, and colloidal chemistry.

The thermodynamic properties of an adsorbate in narrow pores differ appreciably from thermodynamic properties of gases in the bulk phase. The potential of the pore walls changes the conditions of capillary condensation and thus decreases the critical temperature and changes the critical density and pressure.[8–14] At present, adsorption in pores is usually calculated using methods of numerical experiment (MNE)[15–18] and molecular statistics methods, which are based, in particular, on the lattice-gas model (LGM).[19,20] When the potentials of intermolecular interactions are known, the MNE are rather accurate; however, to calculate the properties of systems with trace impurities, one should deal with an enormous number (about 10^4) of molecules of the base component containing a small number of admixed molecules. This hampers obtaining of reliable results in the calculation of the trace impurity distribution. The LGM is an approximate model; nevertheless, it ensures quick solution and does not restrict the amount of trace impurities. The accuracy of the LGM is largely determined by the accuracy of description of the properties of solvents, which influence appreciably the distribution of trace impurities. Comparison of MNE and the LGM shows[13,21–24] that both approaches always give results similar in kind. By modifying the LGM and/or by "adjusting" its energy parameters, one can attain quantitative agreement with virtually exact numerical results obtained by the Monte Carlo and molecular dynamics methods.

The procedure for calculation of adsorption in slit-like pores based on the lattice-gas model is rather simple; it has been considered in detail previ-

Translated from *Izvestiya Akademii Nauk. Seriya Khimicheskaya*, No. 4, pp. 605–615, April, 2000.

1066-5285/00/4904-0609 $25.00

ously.[3,14,21,22,25] In this work, attention is focused on the calculation of the distribution of trace impurities in narrow cylindrical pores in which the wall curvature plays an important role.

The model

The application of the lattice-gas model for describing adsorption in narrow cylindrical pores implies[26] that the pore space can be divided into sites whose volume $V_0 = \lambda^3$ (λ is the lattice constant) is equal to the size of an adsorbed particle. Groups of sites with identical adsorption properties, including those with identical sorbate—sorbent interaction energies Q_q ($1 \le q \le t$, where t is the number of groups of sites in the system), can be distinguished. Let us denote the fraction of sites contained in group q by f_q. Each site can either be occupied by one adsorbed particle or be vacant. Let s be the number of states of occupancy of any site including vacancies. For a one-component fluid $s = 2$, for a base component with an admixture $s = 3$, and for a base component with two admixtures $s = 4$.

Let us consider lattices with the numbers of closest neighbors $z = 6$ and 8. A structure with $z = 6$ provides the best agreement between the theoretically calculated critical parameters and experimental data on these parameters for bulk fluids,[27—29] whereas a structure[23] with $z = 8$ reflects the change in the state of the fluid under the influence of the pore walls. The numerical densities ρ and θ in the MNE[15—18] and LGM,[19—22] respectively, are related to one another by the relation $\rho = \theta(\sigma/\lambda)^3$, where σ is a Lennard—Jones potential parameter corresponding to the diameter of the hard sphere of the particle. The θ value is equal to the ratio of the number of particles to the maximum number of particles possible for the given structure with a constant number of the closest neighbors z. For a rigid incompressible lattice, $\rho = \theta/1.41$, because $\lambda = \sigma(2)^{1/6}$. Then calculations for a lattice with $z = 8$ give the limiting value for the liquid phase to be $\rho = 0.816$ (the result for a lattice with $z = 6$ is $\rho = 0.707$), which is close to $\rho \approx 0.8$ given by the MNE.[23] The use of a structure with $z = 8$ results in a better agreement with the MNE for the liquid-phase branch of the phase diagram of a porous system.[23]

A general approach is demonstrated in relation to argon atoms located as the base component in a graphite pore.

In the case of $z = 6$, one site can be located at the center of a cylindrical pore if $R_p = (h + 0.5)\lambda$ (Fig. 1, *a*) or four sites can be present if $R_p = h\lambda$ (Fig. 1, *b*). Here h is an integer number of lattice constants λ, $h > 1$. Separation of the pore volume into sites and grouping the sites are carried out based on known particle—wall interaction potentials taking into account the symmetry of the inner space of the pore. Figure 1, *a* shows the types of sites with $z = 6$ for a cylindrical pore with $R_p = 4.5\lambda$ and Fig. 1, *c* shows the ones for $z = 8$.

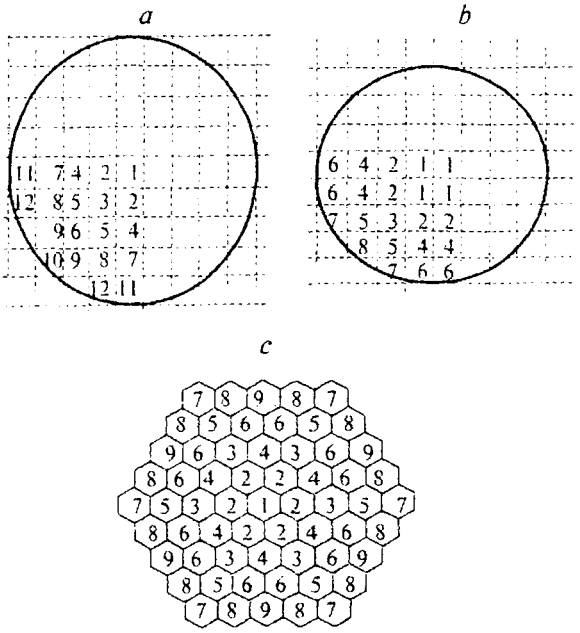

Fig. 1. Cuts of cylindrical pores by lattice structures with $z = 6$ (*a*, *b*) and 8 (*c*). The center of the pore contains one (*a*, *c*) or four (*b*) particles. Numerals denote the numbers of the types of sites (q) into which the pore section is split.

In the lattice model, it is convenient to measure distances in the numbers of coordination spheres r, $1 \le r \le R$. Let us denote the number of sites in an rth coordination sphere surrounding site f by $z_f(r)$; R is the radius of the adsorbate—adsorbate interaction potential. The interparticle interactions are taken into account by energy parameters of the lateral interactions $\varepsilon(r_{ij})$ between particles i and j located in an rth coordination sphere, where $r_{ij} \le R$. In this work, the lattice parameters $\varepsilon(r_{ij})$ were determined from the corresponding distances between the centers of sites located at the distance of the rth coordination sphere using the Lennard—Jones potential: $U_{LJ} = 4\varepsilon_{ij}[(\sigma_{ij}/r_{ij})^{12} - (\sigma_{ij}/r_{ij})^6]$. The value $r_{ij}/\sigma_{ij} = 1.12$ corresponds to the minimum of this potential.

An important characteristic in the LGM is the energy of binding of particle i (i = A, an argon atom, or i = M, an admixed molecule) in site q with the pore walls Q_q^i, which is calculated as

$$Q_q^i = -\beta^{-1} \ln\left\{\frac{1}{V_q}\int_{r\in V_q} \exp[-\beta U_{i-C}(r)]dr\right\}, \quad \beta = 1/(kT), \quad (1)$$

where $U_{i-C}(r)$ is the potential of interaction of particle i with atom C in the pore wall. Integration was performed over the volume $V_q = \lambda^3$ of a cell with number q; $\lambda = 1.12\sigma_{Ar-Ar}$. When the R_p value is fixed, the pore wall intersects some of the cells of the intrapore space. This

is taken into account in the Q_q^i values by decreasing the volume of the cell accessible for the molecule located in the given cell q. Expression (1) giving the parameter Q_q^i ensures agreement of the result obtained in terms of the LGM with the precise result found for a low density of the adsorbate.

The potential of interaction of a particle located at distance y from the cylindrical wall of a pore having the radius R_p was used in the calculations.[23,26]

$$U(y) = -2\pi\varepsilon_{As}n_s\sigma_{As}^2\left[\sum_{j=0}^{\infty}\left(\frac{\sigma_{As}}{R_p + j\Delta - y}\right)^4 f^{(4)}\left(\frac{y}{R_p + j\Delta}\right) - \right.$$

$$\left. - \frac{2}{5}\left(\frac{\sigma_{As}}{R_p - y}\right)^{10} f^{(10)}\left(\frac{y}{R_p}\right)\right], \qquad (2)$$

where Δ is the interlayer spacing in graphite, equal to 0.335 nm; n_s = 38.6 atom nm^{-2} for the basis face of graphite, $\varepsilon_{As} = (\varepsilon_{AA}\varepsilon_{ss})^{1/2}$ and $\sigma_{As} = (\sigma_{AA} + \sigma_{ss})/2$, ε_{ss}/k = 28 K, $\sigma_{AA} = \sigma_{ss}$ = 0.34 nm (the index "s" refers to the carbon atom on the graphite surface and index "A" refers to the adsorbate). Formula (2) is the summation of the interactions of an adsorbate atom with the adsorbent atoms over layers j. The density of the carbon atoms inside each layer j is considered to be uniform. The polynomial coefficients for Eq. (1), $f^{(m)}(x) = \sum_{k=0}^{9} a_{mk}x^k$ for the repulsion (m = 10) and attraction (m = 4) branches of the potential are listed in Table 1. When $R_p \to \infty$, this potential is transformed into the potential for a planar wall.[30] It was assumed that the potential for the interaction of trace impurity M with the wall is described by Eq. (2) with a different parameter ε_{Ms}, which was specified using standard combination rules: $\varepsilon_{Ms} = (\varepsilon_{MM}\varepsilon_{ss})^{1/2}$, $\sigma_{Ms} = (\sigma_{MM} + \sigma_{ss})/2$, and $\varepsilon^* = \varepsilon_{MM}/\varepsilon_{AA}$.

One of the most complicated points in the calculation of the distribution of molecules in pores is calculation of the interface between high- and low-density phases of the adsorbate for capillary condensation below critical temperature. In the case of a single-phase fluid with any pore cross section, shown in Fig. 1, only one distribution of molecules exists. When considering two-phase systems, one should know how the distribution of molecules changes in different pore sections on passing from the low- to high-density phase. At the molecular level, transition from the rarefied to the compact phase occurs as a gradual increase in density through a distance of several lattice constants L rather than as an abrupt jump (L = 1). The region consisting of L intermediate pore sections in which the molecular density develops from that of the rare phase to that of the compact phase is called phase interface; the L value determines its width. Previously this problem has been considered only for a pure fluid in slit-like pores.[22] The L value was determined by its gradual increase up to values such that further increase no longer changed the distribution of molecules in the transient region. No calculations of this type had been carried out for cylindrical pores. Prior to calculations, it is necessary to construct the phase diagram[23,26] for a cylindrical pore of a given width and to determine the local distributions of the fluid over the pore sections in the coexisting low- and high-density phases. These calculations were carried out by a previously reported method.[23,26]

Table 1. Coefficients a_{jk} for the function $f^{(j)}(x)$

k	a_{4j}	a_{10j}	k	a_{4j}	a_{10j}
0	4.71239	7.73126	5	−378.7086	−21794.03
1	−18.84855	−77.08463	6	420.1712	32000.29
2	57.64824	563.1619	7	316.4436	−28996.07
3	−134.9114	−2820.991	8	141.4307	14672.09
4	253.9246	9608.343	9	−27.97551	−3162.542

Equations for the equilibrium distribution of molecules

The partial and full isotherms of a multicomponent mixture of molecules with similar sizes are calculated in terms of the LGM using a cluster approach,[19] which allows one to describe simultaneously the inhomogeneity of adsorption sites and intermolecular interactions in the adsorbate. In the quasi-chemical approximation, the closed set of equations that takes into account direct correlations of interacting particles at distances $r \le R$ has the following form[19]:

$$a_f^i P_i \theta_f^v = \theta_f^i \Lambda_f^i,$$

$$\Lambda_f^i = \prod_r \prod_g \sum_n r_{fg}^{in}(r)\exp[-\beta\varepsilon_{fg}^{in}(r)], \qquad (3)$$

$$^*\theta_{fg}^{ij}(r)\,^*\theta_{fg}^{kn}(r) = {}^*\theta_{fg}^{in}(r)\,^*\theta_{fg}^{jj}(r),$$

$$^*\theta_{fg}^{ij}(r) = \theta_{fg}^{ij}(r)\exp[-\beta\varepsilon_{fg}^{ij}(r)], \qquad (4)$$

where P_i is the partial pressure of adsorptive i in the gas phase; $a_f^i = a_f^{i0}\beta\exp(\beta Q_f^i)$ is the local Henry's constant for molecule i in sites of type f; a_f^{i0} is the preexponential factor for the local Henry constant, a_f^{i0} = 1; for the vacancy (i = v), $a_f^v P_v$ = 1; Λ_f^i is a factor taking account of the lateral interactions of central molecule i in site f with all the closest neighbors. The index f refers to all sites of a lattice structure and index g corresponds to $z_f(r)$ sites of an rth coordination sphere around site f; θ_f^i is the probability that molecule i is located in site f (unary distribution function); $\theta_{fg}^{in}(r)$ is the probability that molecule i is located in site f and molecule n is located in site g at distance r, where $1 \le i, n \le s$ (binary distribution function); $t_{fg}^{ij}(r) = \theta_{fg}^{ij}(r)/\theta_f^i$. The normalizing conditions for the binary ($\theta_{fg}^{in}(r)$) and unary (θ_f^i) distribution functions can be written as follows:

$$\sum_{j=1}^{s}\theta_{fg}^{ij}(r) = \theta_f^i, \qquad \sum_{i=1}^{s}\theta_f^i = 1. \qquad (5)$$

The adsorption isotherm for component i can be calculated from the equation $\theta_i = \sum_{q=1}^{l} f_q \theta_q^i$. For this purpose, set of equations (3)—(5) should first be solved for the local partial coverages of sites θ_q^i. For trace impurities, the form of the set of equations (3) and (4) is simplified because the contributions of trace molecules to the expressions for Λ_f^i can be neglected. Then the dimension of Eqs. (3)—(5) is reduced (down to the dimension of the set of equations for a pure solvent) because the $\theta_{fg}^{in}(r)$ values can be expressed explicitly through the θ_f^A functions

$$\Lambda_f^i = \prod_r \prod_{g \in z_f(r)} |1 + x(r) t_{fg}^{i\Lambda}(r)|,$$

where for a pure solvent,

$$t_{fg}^{AA}(r) = 2\theta_g |\delta_{fg}(r) + b_{fg}(r)|,$$

$$x(r) = \exp[-\beta \varepsilon_{AA}(r)] - 1,$$

$$\delta_{fg}(r) = 1 + x(r)(1 - \theta_f - \theta_g),$$

$$b_{fg}(r) = [\delta_{fg}(r)^2 + 4x(r)\theta_f\theta_g]^{1/2}.$$

Here $\theta_f \equiv \theta_f^A$; for an impurity—solvent pair

$$t_{fg}^{MA}(r) = t_{fg}^{AA}(r)/\{t_{fg}^{AA}(r) + |1 - t_{fg}^{AA}(r)| \times \exp[\beta(\varepsilon_{MA}(r) - \varepsilon_{MA}(r))]\}.$$

The relative distribution of trace impurities for different sites in a pore is of primary interest. Let $\theta_f^i = u_f^i \theta_f^A$, where the function u_f^i is defined as $u_f^i = a_f^i \Lambda_f^A P_i / (P_A a_f^A \Lambda_f^i)$; for $i = A$, we obtain $u_f^i = 1$. Then the $\theta_f^M/\theta_g^M = u_f^M \theta_f^A / u_g^M \theta_g^A$ ratio depends only on the properties of the adsorbate—wall and adsorbate—adsorbate potentials. Hence, the calculation of distribution of a trace impurity in a pore requires only solution of equations for a pure solvent because characteristics of the trace impurity distribution are determined through potential functions and local coverages θ_f^A.

To analyze the properties of the interface, the phase diagram for a cylindrical pore having a fixed width was first calculated. Subsequently the distributions of the low- and high-density phases at the end of region L were considered to be specified, while the distribution of the density of argon atoms in the transient region was calculated from Eqs. (3)—(5), in which the index of site q in expression (1) consists of the number of site f in a given cross section k (as indicated in Fig. 1) and the number of cross section k, $1 \le k \le L$. We performed calculations for different lattice structures with $z = 6$ and 8 and different radii of lateral interaction, $R = 1\lambda$ and 4λ. The distribution of a pure fluid (the base component) and trace impurities was considered taking ε^* to be 0.5 (weakly interacting impurity) and 2.0 (strongly interacting impurity). The change in ε^* changes simultaneously the energy of the adsorbate—adsorbate lateral interactions and, according to Eq. (2), the adsorbate—adsorbent interaction energy. The results are given for a fixed pore radius, $R_p = 4\lambda$.

Molecule distributions

The results of calculation of the distribution of molecules at the interface between the high- and low-density phases of the adsorbate in a cylindrical pore at $T/T_c = 0.8$, where T_c corresponds to the bulk gas phase, are presented in Fig. 2 for two lattice structures with $z = 6$ (*a*) and 8 (*b*). Due to the adsorption potential of the walls, the phase diagrams of porous systems differ from those of bulk phases: in particular, critical temperature decreases.[8—14] The T_c value depends on the type of the lattice structure z, because this determines the number of neighboring molecules, which "counterbalance" the kinetic energy of the molecules.

Figure 2 presents contour lines for equal density of molecules for pure components (*a*, *d*) and for weakly and strongly interacting trace impurities (*b*, *c* and *e*, *f*). For clarity, Fig. 2 presents smoothed values, instead of the discontinuous changes of the local densities θ_q^i in different structure sites, whose sections are shown in Fig. 1. They were obtained by constructing the projection of θ_q^i along the pore radius in a chosen direction. In this study, these directions connect sites 1 and 11 in Fig. 1, *a* (structure with $z = 6$) and sites 1 and 7 in Fig. 1, *c* (structure with $z = 8$). Then the computer graphics is smoothed using the quadratic procedure. The contour lines for a pure solvent show real molecule densities expressed in dimensionless values θ. These curves resemble the curves of distribution of molecules in slit-like pores.[22] The values of density for a trace impurity are normalized by the gas density outside the pore.

The structure of the phase boundary between the low- and high-density phases determines the distribution of the base component; therefore, the contour lines are similar in shape to the phase boundary for argon atoms. It can be clearly seen that the phase boundary extends for about six monolayers. (Note that, as in the case of slit-like pores,[22] an increase in the temperature widens the phase boundary.) The central part of the Figure corresponds to the low-density ("gas") phase, while the "liquid" phase is located at the edges. The cross-sections of the volumes occupied by the gas and liquid phases reflect the pattern of the layer-by-layer variation of coverage in these phases. In the gas phase, a dense "film" (about two monolayers) of adsorbed molecules is located near the wall. A weakly interacting impurity is accumulated on the walls to a lesser degree than a strongly interacting impurity. The former can be easily "displaced" from the walls by argon atoms, whereas the latter is retained at the walls even when the density

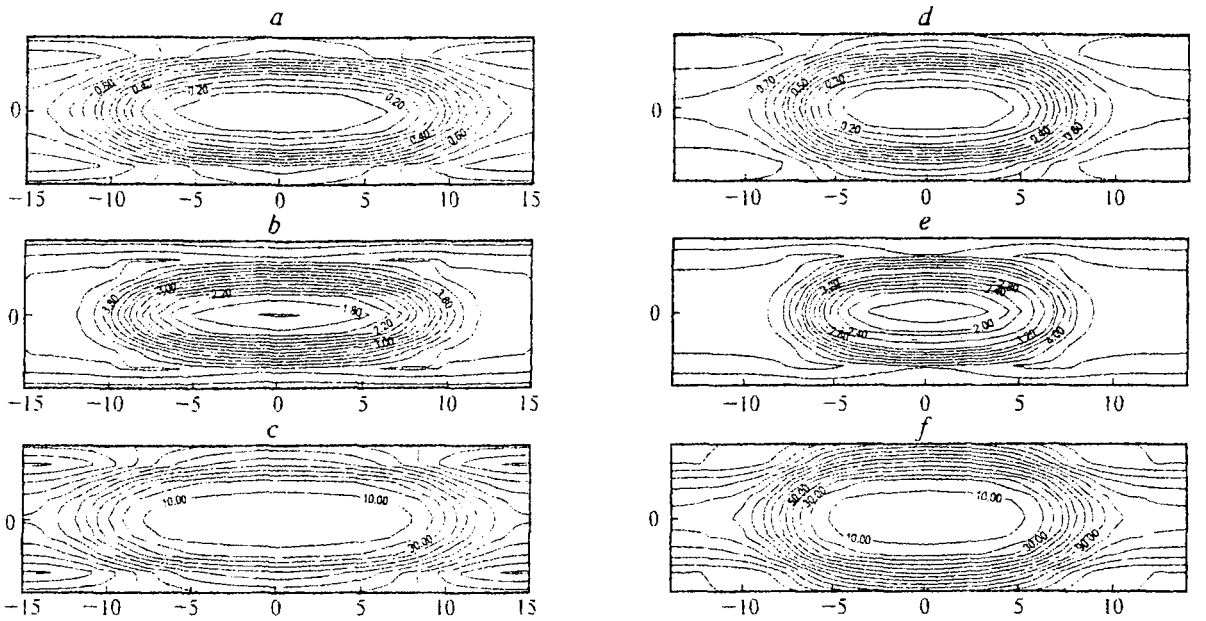

Fig. 2. Density contour lines at the interface between the high- and low-density phases in a cylindrical pore. Calculations for a lattice structure with $z = 6$ (*a*—*c*) and 8 (*d*, *e*). The abscissa corresponds to a pore section with a length of 27 sites and the ordinate axis corresponds to the pore diameter; (*a*, *d*) distribution of the base component at $T/T_{crit} = 0.8$; (*b*, *e*) distribution of a weakly interacting trace impurity, $\varepsilon^* = 0.5$; (*c*, *f*) distribution of a strongly interacting trace impurity, $\varepsilon^* = 2.0$.

of the base component is high. The distribution patterns of trace impurities for the two lattice structures are similar. The quantitative distinctions are due first of all to different critical temperatures of the two structures in the bulk gaseous phases (T_c for $z = 6$ is lower than T_c for $z = 8$, and the ratio under study, $T/T_c \approx$ const). In addition, when the cylinder radius is small and, hence, a pore cross section accommodates a small number of sites, the distribution of sites between the near-wall and central parts of a pore starts to play a role. However, due to the smoothed character of the curves presented in Fig. 2, the latter factor is less significant than the former one.

The process of redistribution of a trace impurity between the wall (θ_{2w}) and the center (θ_{2c}) of the pore is characterized quantitatively by the selectivity coefficient

$$S = \theta_{2c}/\theta_{2w}. \qquad (6)$$

Let is consider the analytical estimates for the function S for low ($\theta_1 \approx 0$), critical (θ_{crit}), and large ($\theta_2 \approx 1$) pore coverages. Index 1 refers to the base component, 2 corresponds to an impurity, and 3 denotes a vacancy.

Let us rewrite Eq. (6) in the following form

$$S = a_{2c}\theta_{3c}\Lambda_{2w}/a_{2w}\theta_{3w}\Lambda_{2c}, \qquad (6a)$$

where a is Henry's constant and Λ is the nonideality function. Taking into account the combination rules, we found that $\varepsilon_{1w} = (\varepsilon_{11}\varepsilon_{ww})^{1/2}$ and $\varepsilon_{2w} = (\varepsilon_{22}\varepsilon_{ww})^{1/2} = \varepsilon_{1w}(\varepsilon^*)^{1/2}$, and $\varepsilon_{21} = \varepsilon_{12} = (\varepsilon_{11}\varepsilon_{22})^{1/2} = \varepsilon_{11}(\varepsilon^*)^{1/2}$, where $\varepsilon^* = \varepsilon_{22}/\varepsilon_{11}$, $\varepsilon^* = 0.5$, 1.0, 2.0.

1. For low density, $\theta_1 \approx 0$, we obtain $\theta_{3c} = \theta_{3w} = 1$ and $\Lambda_{2w} = \Lambda_{2c} = 1$. By substituting successively these values for local θ and Λ, we found

$$S = a_{2c}\theta_{3c}\Lambda_{2w}/a_{2w}\theta_{3w}\Lambda_{2c} = \exp[-\beta(\varepsilon_{2w} - \varepsilon_{2c})] \approx \exp(-\beta\varepsilon_{2w}),$$

because $a_{2w} = a_0\exp(-\beta\varepsilon_{2w})$ and $a_{2c} = a_0\exp(-\beta\varepsilon_{2c})$, where $\varepsilon_{2c} \approx 0$.

Finally,

$$\beta\varepsilon_{2w} = \beta\varepsilon_{1w}(\varepsilon^*)^{1/2}$$

$$\text{and } S(\theta_1 \approx 0) = \exp[-\beta\varepsilon_{1w}(\varepsilon^*)^{1/2}]. \qquad (6b)$$

It follows from this result that the greater ε^*, the smaller the selectivity coefficient for zero coverages.

2. In the case of critical coverages, the overall θ_{crit} values[13,14,23,25] are ~0.7—0.8. The local values of free sites are $\theta_{3c} = (1 - \theta_{1c}) \approx 0.5$ and $\theta_{3w} = (1 - \theta_{1w}) \approx 0.01$—$0.0001$.

To estimate S, we use the expression for the function Λ in the mean-field approximation[19]: $\Lambda_{2w} = \exp[-\beta\varepsilon_{21}(z\theta_1)_w]$ and $\Lambda_{2c} = \exp[-\beta\varepsilon_{21}(z\theta_1)_c]$. Taking into account the facts that the density on the wall $(\theta_{crit})_w$ is close to unity, the density in the inner layers of a pore $(\theta_{crit})_c$ is about 0.5, and the numbers of neighboring sites for a site in the bulk ($z_c = 6$) and one near the wall ($z_w = 4$) are different, we have

$$S(\theta_{crit}) = \exp[-\beta\varepsilon_{1w}(\varepsilon^*)^{1/2}][(1 - \theta_{1c})/(1 - \theta_{1w})]\times$$

$$\times\exp\{\beta\varepsilon_{21}[(z\theta_1)_c - (z\theta_1)_w]\}.$$

By substituting the above θ and z values into this expression, we obtain

$$S(\theta_{crit}) = \exp[-\beta\varepsilon_{1w}(\varepsilon^*)^{1/2}][10^2-10^4]\times$$

$$\times\exp\{\beta\varepsilon_{21}[(6\cdot 0.5)_c - (4\cdot 1)_w]\} =$$

$$= \exp[-\beta\varepsilon_{1w}(\varepsilon^*)^{1/2}][10^2-10^4]\exp[-\beta\varepsilon_{11}(\varepsilon^*)^{1/2}]. \quad (6c)$$

This expression shows that under the near-critical conditions, $S(\theta_{crit}) > S(\theta_1)$ and that the S value decreases as ε^* increases. In the critical region, when the attraction of atoms to the walls is fairly strong, S cannot be greater than ten. (Note that in our estimates, the $[(1-\theta_{1c})/(1-\theta_{1w})]$ ratio is fixed and does not depend on ε^*.)

3. In the case of high density, full coverage of the pore corresponds to $\theta_2 \approx 1$ when each local density tends to unity.

As a consequence, the $[(1-\theta_{1c})/(1-\theta_{1w})]$ ratio remains almost the same as in the critical region (10^2—10^4) but the ratio of the terms in the exponent changes

$$S(\theta_2) = \exp[-\beta\varepsilon_{1w}(\varepsilon^*)^{1/2}][10^2-10^4]\exp\{\beta\varepsilon_{21}[(z\theta_1)_c - (z\theta_1)_w]\} =$$

$$= \exp[-\beta\varepsilon_{1w}(\varepsilon^*)^{1/2}][10^2-10^4]\exp[\beta\varepsilon_{11}(\varepsilon^*)^{1/2}\theta_1\Delta z], \quad (6d)$$

because $\theta_{1c} \approx \theta_{1w} \approx 1$ and $\Delta z = z_c - z_w > 0$ (for any z). This indicates that an increase in the density induces an increase in the selectivity, which becomes more and more pronounced as ε^* grows. Thus, the ε^* value is still significant and determines the limiting value of the function $S(\theta_2)$ even for full coverage of the pore.

These qualitative estimates are confirmed by calculation of the selectivity coefficient of trace impurity located between the pore center and the wall (Fig. 3). The curves for the variation of $\ln S$ *vs* volume filling of a pore show qualitatively similar patterns for any impurity (the character of impurity is determined by the parameter ε^*). When the pore coverage with the base component increases, the coverage of the first layer is the first to increase and the neighboring adsorbed molecules hold the impurity more strongly near the wall due to lateral interactions; therefore, the curve for $\ln S$ *vs* $P/(kT)$ has a minimum. However, further increase in the pore coverage results in the impurity being displaced from the walls to the bulk of the pore by the great amount of the base component. When the near-surface region of the pore is fully covered (this is about two surface monolayers), the function S sharply increases. This behavior is manifested as a rule in the near-critical region, in which the pore surface is covered almost completely (provided that the molecules are strongly attracted by the walls, as we assume here) and the volume of the pore is filled approximately by half with the base component. Further filling of the pore bulk has only a slight influence on the S value. The stronger the interaction of the impurity with the walls and with the base component molecules, the stronger the impurity is held by the walls and the lower the selectivity coefficient at any pore coverage.

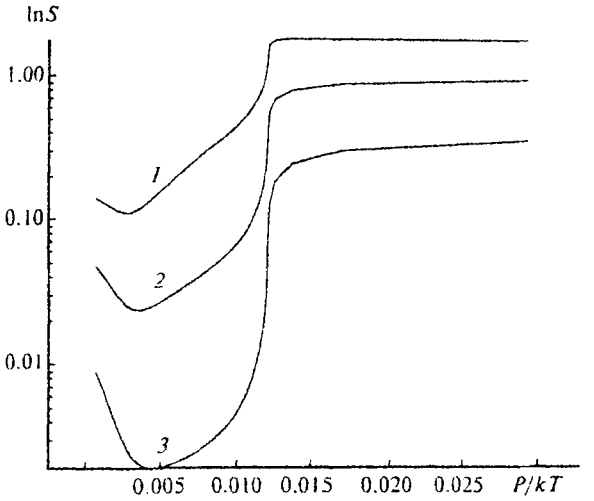

Fig. 3. Coefficient of distribution of a trace impurity between the pore bulk and the pore wall (S) for the case of $R = 1\lambda$, $z = 6$ as a function of the degree of filling of the pore volume with the solvent (the P/kT values for the gas phase are laid off on the abscissa) for a weakly interacting impurity (*1*), the base component (*2*), and a strongly interacting impurity (*3*).

Self-diffusion coefficients

With a knowledge of the equilibrium distribution of particles, it is possible to determine self-diffusion coefficients.[19,31] In the case of narrow pores, the self-diffusion coefficient characterizes the thermal motion of molecules along the pore axis. The expression for the self-diffusion coefficient of molecules i, where i is the label of either the base component or trace impurity, provided that they show an equilibrium distribution over the pore cross section, is written[31] as

$$D_i^* = \lambda^2 \sum_{q=1}^{t} \tilde{z}_q f_q \sum_{p=1}^{t} d_{qp}(V_{qp}^i/\theta_q)\, d\theta_q^{*i}/d\theta_i^*. \quad (7)$$

$$V_{qp}^{iN} = K_{qp}^{iN}\theta_{qp}^{iN}\Lambda_{qp}^{iN}. \qquad \Lambda_{qp}^{iN} = \prod_{r=1}^{R}\prod_{\omega_r}\prod_{h} S_{qph}^{iN}(\omega_r).$$

When deriving this expression,[31] the researchers used a transition state model taking into account all the jumps of a migrating molecule into neighboring sites of various types. Averaging was performed for both the contributions of sites to which the molecule migrates (type p sites) and the contributions of sites from which it migrates (type q sites). Here V_{qp}^{iN} is the rate of migration of molecule i from a type q site into a type p site; $K_{qp}^{iN} = K^*{}_{qp}^{iN}\exp(-\beta E_{qp}^{iN})$ is the rate constant for the migration of molecule i from site q into a vacant site p; E_{qp}^{iN} is the activation energy of migration; $K^*{}_{qp}^{iN} = F_i^*/(h\beta F_i)$ is the preexponential factor for the rate constant, h is the Planck constant; and F_i^* and F_i are the

statistical sums for particle i in the transition and ground states; for the distributed model considered, $d_{qp} = 1/z_q$. The effect of interparticle interactions on the activated migration is determined by the function Λ_{qp}^{iv}.

$$S_{qp\Lambda}^{iv}(\omega_r) = \sum_{j=\Lambda}^{V} T_{qph}^{ivj}(\omega_r) E_{qph}^{ivj}(\omega_r),$$

$$T_{qph}^{ivj}(\omega_r) = \theta_{qh}^{ij}(r_1)\theta_{ph}^{vj}(r_2)/(\theta_q^i\theta_p^v\theta_h^j),$$

$$E_{qph}^{ivj}(\omega_r) = \exp\{\beta[\delta\varepsilon_{qh}^{ij}(r_1) + \delta\varepsilon_{ph}^{vj}(r_2)]\},$$

$$\delta\varepsilon_{qh}^{ij}(r) = \varepsilon^*{}_{qh}^{ij}(r) - \varepsilon_{qh}^{ij}(r).$$

During migration, the moving particle is subject to the influence of neighboring particles; the energy of this interaction is described by the parameters $\varepsilon^*{}_{qh}^{ij}(r)$, which differ from the corresponding energy parameters for particles in the ground state, $\varepsilon_{qh}^{ij}(r)$. The particles surrounding the activated complex can be conveniently numbered using the numbers of sites $h \in m(\omega_r)$ having different orientations ω_r ($1 \le \omega_r \le \pi_r$), where π_r is the number of orientations in an rth common coordination sphere about dimer iv at central sites q and p (*i.e.*, for sites located at distance r from either site q or site p). The orientations are referred to the center of dimer iv, *i.e.*, the point of intersection of the line connecting the central sites with the line connecting site h with the dimer center.

To calculate the derivative $d\theta_q^{*i}/d\theta_i^*$ in Eq. (7), we take into account that $\theta_i^* = \sum_{q=1}^{t} f_q \theta_q^{*i}$; therefore,

$$d\theta_q^{*i}/d\theta_i^* = (d\theta_q^{*i}/d\theta)/(d\theta_i^*/d\theta) = [(du_q^i/d\theta)\theta_q^i +$$

$$+ u_q^i(d\theta_q^i/d\theta)]/\{\sum_q f_q [(du_q^i/d\theta)\theta_q^i + u_q^i(d\theta_q^i/d\theta)]\}.$$

The rate constants for migration from different sites comply with a simple condition: the deeper the well, the lower the probability that a particle would leave it. The relationship between the migration constants and local Henry's constants has the following form: $a_q^i K_{qp}^{iv} = a_p^i K_{pq}^{iv}$, which takes into account that $a_q^i = a_q^{0i}\exp(\beta Q_q^i)$. It was assumed in calculations that $E_{qp}^{iv} = \gamma Q_q^i$, $\gamma = 1.1$ (if $Q_q^i \ge Q_p^i$) and $\varepsilon^*{}_{qh}^{ij}(r) = \varepsilon^*{}_{ij}(r)$, $\varepsilon_{qh}^{ij}(r) = \varepsilon_{ij}(r)$ for any type of structure sites.

The general trend for the self-diffusion coefficients of molecules to decrease with an increase in the degree of pore coverage is due to the decrease in the free space accessible for molecules (Fig. 4). The pattern of concentration dependence of $D_i^*(\theta)$ for the base component depends substantially on the ratio of the lateral interactions of molecules in the ground and transition states. If the difference between the interactions of molecules in the ground and transition states can be neglected, the concentration dependence of the self-diffusion coefficient monotonically decreases. The slope of the curve for $D_i^*(\theta)$ at low coverages is much greater than that for near-critical coverages. This behavior of $D_i^*(\theta)$ at low coverages is due to the increase in the fraction of molecules located in the central part of the pore, in which these molecules migrate faster than near the pore walls. The decrease in $D_i^*(\theta)$ at high coverages is associated with the dramatic decrease in the proportion of vacancies. For $z = 6$ and $R = 1\lambda$, it is sufficient that $\alpha = \varepsilon_{AA}^*(1)/\varepsilon_{AA}(1) > 0.1$ for the pattern of the monotonic decrease in $D_i^*(\theta)$ for near-critical coverages to change due to the enhancement of the lateral attraction in the transition state. For other z and R values, the α value corresponding to a nonmonotonic variation of $D_i^*(\theta)$ is greater than 0.1, but the above-mentioned feature remains qualitatively the same.

Figure 5 shows analogous plots for the self-diffusion coefficients of weakly (*a*) and strongly (*b*) interacting trace impurities. (The curves were normalized by the self-diffusion coefficient of the solvent label for zero coverage.) The pattern of the concentration curves for the self-diffusion coefficients is generally retained. The family of curves for weakly interacting impurities shifts to higher self-diffusion coefficients with respect to the label of the solvent. However, in all cases, an increase in α brings about a nonmonotonic variation of $D_i^*(\theta)$.

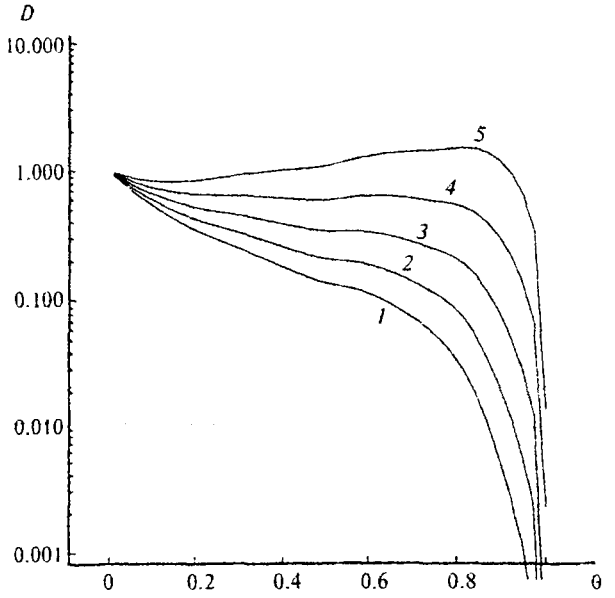

Fig. 4. Concentration dependences of the self-diffusion coefficient (D) for the base component for $z = 6$, $R = 1\lambda$, and the parameter $\alpha = 0$ (*1*), 0.05 (*2*), 0.10 (*3*), 0.15 (*4*), 0.20 (*5*).

The curves for other molecular parameters ($z = 8$ and $R = 4$) are shown in Fig. 6 in a linear scale along the ordinate axis. For weakly interacting impurities, the first local maximum can be observed at low coverages, and the second local maximum can occur at a near-critical coverage. In the case of strongly interacting impurities, no maximum is observed at low coverages, the impurity is located near the walls, and migration through the pore center makes a low contribution. In the case of a weakly interacting impurity, the fraction of molecules in the pore bulk is much greater than that near the walls. The fraction of this component in the pore bulk increases with an increase in the concentration of the base component. This accounts for the presence of the first local maximum.

It can be seen in Figs. 5 and 6 that the maximum at greater θ is due to two reasons: (1) the difference between the interactions of a migrating particle with the environment in the ground and transition states and (2) the increase in the concentration of the base component to near-critical values. When the concentration of the base component increases, the trace component is displaced from the walls to the pore bulk, where it moves more vigorously; however, the maximum of $D_i^*(\theta)$ is displayed only provided that the relationship α(impurity) > α(solvent) holds. Thus, the concentration dependences of the self-diffusion coefficients are highly sensitive to the potential of intermolecular interactions for the base component and depend appreciably on the total concentration of this component. Further increase in the density of the base component decreases the mobility of both this component and any impurity.

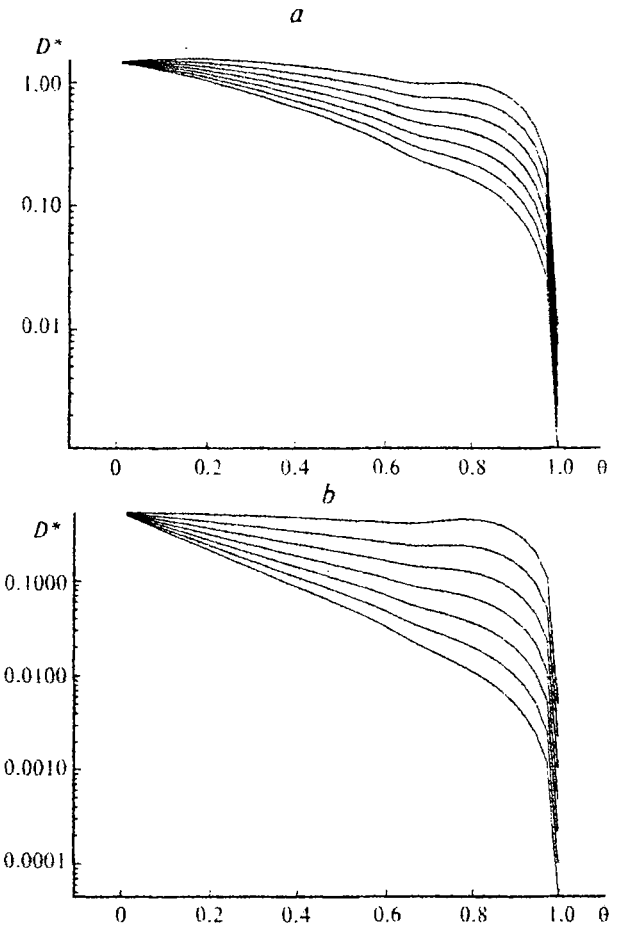

Fig. 5. Concentration dependences of the self-diffusion coefficient of weakly (*a*) and strongly (*b*) interacting impurities at $z = 6$, $R = 4\lambda$. The parameter α (for the base component) = 0.5; α (for the impurity) changes from the lower to the upper curve from −1.0 to 1.0 with a step of 1/3.

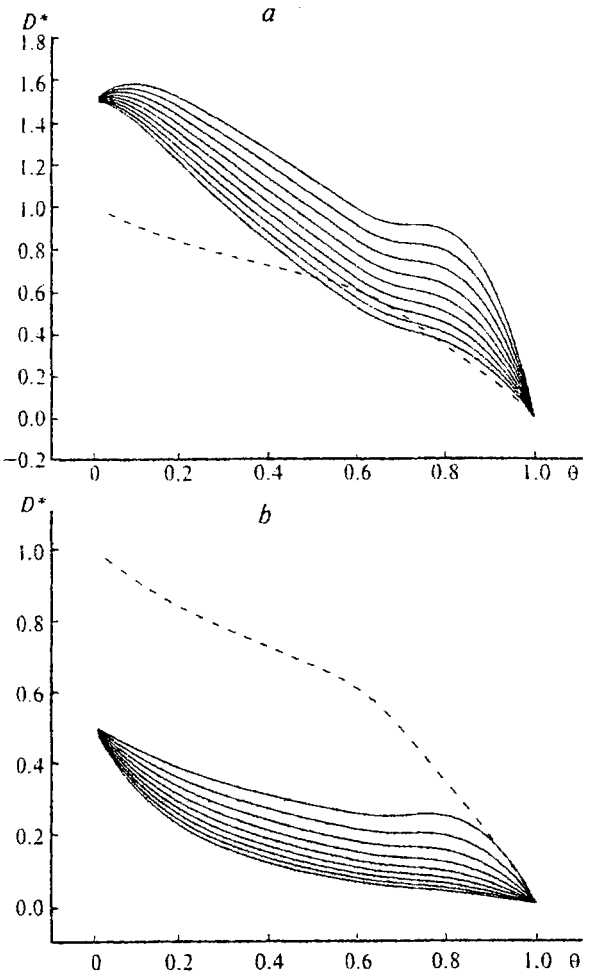

Fig. 6. Concentration dependences of the self-diffusion coefficient of weakly (*a*) and strongly (*b*) interacting impurities for $z = 8$, $R = 4\lambda$. The parameter α (for the base component) = 0.6; α (for the impurity) changes from the lower to the upper curve from 0.4 to 0.8 with a step of 0.05 (the dashed line shows the curve for the base component).

The distributions of clusters

Let us consider the distribution of clusters in cylindrical pores depending on the degree of pore coverage by the main component. The atoms in clusters are mainly connected* due to van der Waals forces. The energy of bond cleavage in these clusters is relatively low; therefore, the concentration of clusters in gases under normal conditions is low. However, as the temperature decreases, the concentration of clusters always increases. In porous systems, this concentration also depends on the parameters of interaction of particles with the wall and on the geometrical size of the micropores because the bulk phase diagram changes appreciably under the influence of pore walls[8—14,23,25,32] and, correspondingly, the regions of existence of the supersaturated state of the fluid sharply change compared to those in the bulk phase.

The distribution of clusters consisting of atoms of different sorts depends on the mutual attraction or repulsion of these atoms. The distribution of clusters containing trace impurities depends substantially on the concentration of the base component. It is these distributions of clusters that govern the processes of homogeneous catalysis in solutions and the possible degree of limiting exhaustion of various reactants in these processes.[33—35] Similar processes in microporous systems can play an important role provided that both reactants are adsorbed by the adsorbent. In this case, the effect of the adsorption field can sharply change (either increase or decrease) the proportions of clusters of different types in various pore cross sections with respect to the volume distribution of clusters; correspondingly, the probabilities of participation of these components in reactions also change.

The lattice model permits effective analysis of the distribution of clusters in micropores. By analogy with the gas phase, a cluster of size n in a pore is an isolated particle consisting of n atoms linked to one another by at least one bond and surrounded by vacant sites of the lattice.[32] The vacancies ensure the isolation of the particle. The atoms in the cluster can be arranged in different ways depending on the number of inner bonds. The clusters in pores are formed from atoms located in different groups of sites. Therefore, the equilibrium concentrations of clusters depend on the position of their center of gravity with respect to the perpendicular to the wall surface and on the cluster orientation with respect to the perpendicular. With known local coverages of sites of various types θ_f, one can calculate the equilibrium probabilities of the formation of clusters $\theta_{clus}(n|f)$ of size n having a center of gravity in a type f site or the concentrations of these clusters: $\theta_{clus}(n|f) = \theta(n|f)\Phi(n|f)$, where $\theta(n|f)$ is the probability that monomers of various sorts fill a certain group of n sites linked to one another and having a center of gravity in a site of type f, and $\Phi(n|f)$ is the probability of existence of many vacant sites surrounding the given set of atoms in the cluster. The possibility of calculation of the concentrations of clusters for various degrees of coverage of a cylindrical pore is illustrated below in relation to dimeric clusters containing foreign atoms of various sorts.

Analysis of the probabilities of the formation of clusters of various sizes from the base component (argon) as functions of the position of the center of gravity of clusters relative to the walls of slit-like and cylindrical pores at various degrees of coverage of the micropores[26,32] resulted in the following conclusions: (1) the patterns of these curves depend substantially on the type of interactions of molecules with the pore walls. In the case of unwettable pores, which a sort of "repel" argon atoms, the cluster stability inside pore is determined by interatomic interactions. Conversely, in the case of readily wettable walls, which strongly "attract" argon atoms, all the cluster atoms tend to be located near the wall forming a planar configuration; (2) the equilibrium concentrations of clusters in the pores change dramatically upon change in the cluster positions in the pore bulk and the orientation relative to the pore wall; (3) as the degree of filling of the pore volume increases, the concentrations of various clusters sharply decrease.

The quantitative differences between equally wide slit-like and cylindrical pores are due to the increase in the proportion of sites in the near-wall region and to the decrease in the proportion of sites in the bulk of the pore in the case of cylindrical pores.

Figure 7 presents the concentration dependences of the formation of cluster dimers whose orientations relative to the pore walls are specified by the numbers of central sites (f—g). The probabilities of the existence of dimers formed from monomers i and j located in neighboring sites f and g (see Fig. 1, *a*, *c*) are expressed as

$$\theta_{clus}^{ij}(2|fg) = \theta_{ij}(2|fg)\Phi_{ij}(2|fg),$$

where

$$\theta_{ij}(2|fg) = \theta_f^i t_{fg}^{ij}, \qquad \Phi_{ij}(2|fg) = \prod_{h \in z_{fg}(1)} t_{fgh}^{ijv},$$

$$t_{fgh}^{ijv} = \theta_{fh}^{iv}\theta_{gh}^{jv}/(\theta_f^i\theta_g^j\theta_h^v).$$

Here, site h implies all the closest neighbor sites surrounding the central pair of sites fg; the number of these sites is denoted by $z_{fg}(1)$.

Figure 7 presents the variation of the probability of dimer formation *vs* the degree of coverage of a cylindrical pore with readily wettable walls (lattice structure with $z = 8$). The following designations were introduced for the system components: B is the base component and W and S are weakly and strongly interacting impurities, respectively. The curves in Figs. 7, *a* and 7, *b* refer to different sorts of dimers in sites (f—g) in the

* This refers to weakly bound groups of adsorbate atoms or molecules rather than coordination compounds, whose molecules are formed by strong chemical bonds of the metal—metal type.

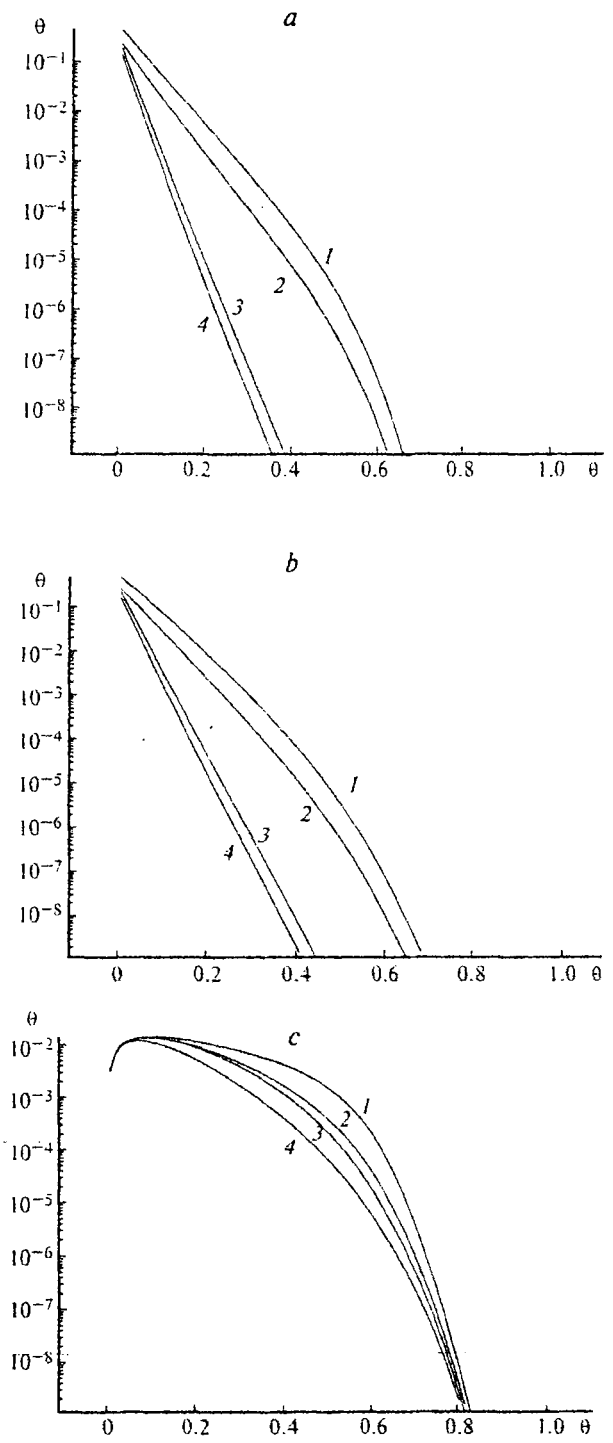

Fig. 7. Concentration dependences of the distributions of dimeric clusters (θ) inside a cylindrical pore (temperature $T = 1.01T_{crit}$): (*a* and *b*) the (1—2) and (3—4) pairs of sites, respectively, containing different atoms forming the following dimers in the ternary system: (*1*) WW, (*2*) SW, (*3*) WS, (*4*) SS; (*c*) the dimer BW formed by the base component in site *f* and the weakly interacting impurity in site *g* for the following pairs of sites (*f*—*g*): (*1*) (1—2), (*2*) (2—3), (*3*) (3—4), (*4*) (4—6).

pore bulk, namely, the (1—2) and (3—4) pairs of sites (see Fig. 1, *c*). In the general case, the cluster concentrations decrease with an increase in the volume filling of the pore. However, the region of concentrations of the base component in which the dimer concentration noticeably differs from zero depends appreciably on the nature of the monomer and on the cluster orientation. Comparison of the curves corresponding to dimers formed from weakly interacting monomers with similar curves for dimers formed by strongly interacting impurities shows that the concentrations of weakly interacting impurities decrease more slowly with an increase in the degree of filling. This is due to the displacement of "weak" dimers to the pore bulk, which is filled only after the near-surface region has been covered.

The curves presented in Fig. 7, *c* correspond to a dimer formed by molecules of the base component and a weakly interacting impurity located in different positions inside the pore, namely, the (1—2), (2—3), (3—4), and (4—6) pairs of sites. In this case, nonmonotonic variation is observed; the dimer concentrations first increase and then decrease. The closer to the wall are the dimers, the more rapidly their concentration decreases because the near-wall region is covered predominantly.

The analysis performed showed that the general features of distribution of isolated clusters in various points inside narrow pores, found previously[26,32] for molecules of the base component, are also valid for clusters formed by impurity molecules. However, the nature of the impurity molecule can substantially influence the probability of formation of various types of mixed clusters and their orientation relative the pore walls.

This work was financially supported by the INTAS and by the Russian Foundation for Basic Research (Project No. 95-116).

References

1. D. M. Ruthven, *Principles of Adsorption and Adsorption Processes*, J. Wiley, New York, 1984.
2. S. F. Timashev, *Fiziko-khimiya membrannykh protsessov* [*Physical Chemistry of Membrane Processes*], Khimiya, Moscow, 1988, 237 pp. (in Russian).
3. T. A. Kuznetsova, A. E. Sigaeva, and A. M. Tolmachev, *Vestn. Mosk. Univ., Ser. Khimiya*, 1988, **29**, 43 [*Bull. Mosc. Univ.*, 1988 (Engl. Transl.)].
4. M. F. Gilyazov, A. A. Lopatkin, and A. M. Tolmachev, *Vysokochistye Veshchestva*, 1987, No. 6, 40; 48 [*High-Purity Substances*, 1987, No. 6 (Engl. Transl.)].
5. Yu. K. Tovbin, M. F. Gilyazov, and A. M. Tolmachev, *Vysokochistye Veshchestva*, 1990, No. 1, 76; 83 [*High-Purity Substances*, 1990, No. 1 (Engl. Transl.)].
6. S. J. Gregg and K. S. W. Sing, *Adsorption, Surface Area, and Porosity*, Academic Press, London, 1982.
7. A. V. Kiselev, *Mezhmolekulyarnye vzaimodeistviya v adsorbtsii i khromatografii* [*Intermolecular Interactions in Adsorption and Chromatography*], Vysshaya Shkola, Moscow, 1986, 360 pp. (in Russian).

8. M. E. Fisher and H. Nakanishi, *J. Chem. Phys.*, 1981, **75**, 5857.
9. H. Nakanishi and M. E. Fisher, *J. Chem. Phys.*, 1983, **78**, 3279.
10. P. Tarasona, U. M. B. Marconi, and R. Evans, *Mol. Phys.*, 1987, **60**, 573.
11. E. Bruno, U. M. B. Marconi, and R. Evans, *Physica A*, 1987, **141**, 187.
12. A. de Kreizer, T. Michalski, and G. H. Findenegg, *Pure Appl. Chem.*, 1991, **63**, 1495.
13. Yu. K. Tovbin and E. V. Votyakov, *Langmuir*, 1993, **9**, 2652.
14. E. V. Votyakov and Yu. K. Tovbin, *Zh. Fiz. Khim.*, 1994, **68**, 287 [*Russ. J. Phys. Chem.*, 1994, **68** (Engl. Transl.)].
15. D. V. Fedoseev, R. K. Chuzhko, and A. G. Grivtsov, in *Geterogennaya kristallizatsiya iz gazovoi fazy* [*Heterogeneous Crystallization from the Gas Phase*], Nauka, Moscow, 1978, p. 60 (in Russian).
16. D. Nicolson and N. G. Parsonage, *Computer Simulation and the Statistical Mechanics of Adsorption*, Academic Press, New York, 1982.
17. E. N. Brodskaya and E. M. Piotrovskaya, *Rasplavy* [*Melts*], 1988, **2**, 29 (in Russian).
18. Yu. K. Tovbin, in *Metod molekulyarnoi dinamiki v fizicheskoi khimii* [*Molecular Dynamics Method in Physical Chemistry*], Nauka, Moscow, 1996, p. 128 (in Russian).
19. Yu. K. Tovbin, *Theory of Physicochemical Processes at the Gas–Solid Interface*, CRC Press, Boca Raton, Fl., 1991.
20. Yu. K. Tovbin, *Progress in Surfaces Sci.*, 1990, **34**, 1.
21. Yu. K. Tovbin, *Langmuir*, 1997, **13**, 979.
22. Yu. K. Tovbin and T. V. Petrova, *Zh. Fiz. Khim.*, 1995, **70**, 127 [*Russ. J. Phys. Chem.*, 1995, **70** (Engl. Transl.)].
23. E. V. Votyakov, Yu. K. Tovbin, J. M. D. Macelroy, and A. Roche, *Langmuir*, 1999, **15**, 5713.
24. Yu. K. Tovbin, *Zh. Fiz. Khim.*, 1998, **72**, 2280 [*Russ. J. Phys. Chem.*, 1998, **72** (Engl. Transl.)].
25. Yu. K. Tovbin and E. V. Votyakov, *Zh. Fiz. Khim.*, 1993, **67**, 2126 [*Russ. J. Phys. Chem.*, 1993, **67** (Engl. Transl.)].
26. Yu. K. Tovbin and E. V. Votyakov, *Zh. Fiz. Khim.*, 1998, **72**, 1885 [*Russ. J. Phys. Chem.*, 1998, **72** (Engl. Transl.)].
27. T. L. Hill, *Statistical Mechanics: Principles and Selected Applications*, McGraw-Hill, New York, 1956.
28. J. O. Hirschfelder, C. F. Curtiss, and R. B. Bird, *Molecular Theory of Gases and Liquids*, J. Wiley and Sons, New York, 1954.
29. O. Yu. Batalin, Yu. K. Tovbin, and V. K. Fedyanin, *Zh. Fiz. Khim.*, 1980, **53**, 3020 [*Russ. J. Phys. Chem.*, 1980, **53** (Engl. Transl.)].
30. W. A. Steele, *The Interactions of Gases with Solid Surfaces*, Pergamon, New York, 1974.
31. Yu. K. Tovbin, *Dokl. Akad. Nauk SSSR*, 1990, **312**, 918 [*Dokl. Chem.*, 1990 (Engl. Transl.)].
32. Yu. K. Tovbin, V. N. Komarov, and N. F. Vasyutkin, *Zh. Fiz. Khim.*, 1999, **73**, 500 [*Russ. J. Phys. Chem.*, 1999, **73** (Engl. Transl.)].
33. D. M. Pfund, L. L. Lee, and H. D. Cochran, *J. Chem. Phys.*, 1991, **94**, 3114.
34. R.-S. Wu, L. L. Lee, and H. D. Cochran, *Ind. Eng. Chem. Res.*, 1990, **29**, 977.
35. A. A. Chialo and P. G. Debenedetti, *Ind. Eng. Chem. Res.*, 1992, **31**, 1391.

Received April 27, 1999;
in revised form July 13, 1999